Int J Adv Manuf Technol (2009) 42:621–632
DOI 10.1007/s00170-008-1627-x

ORIGINAL ARTICLE

Study on orthogonal turning of titanium alloys with different coolant supply strategies

Z. G. Wang · M. Rahman · Y. S. Wong · K. S. Neo · J. Sun · C. H. Tan · H. Onozuka

Received: 2 April 2008 / Accepted: 17 June 2008 / Published online: 22 July 2008

Abstract In this paper, the effects of different coolant supply strategies (using flood coolant, dry cutting, and minimum quantity of lubricant [MQL]) on cutting performance in continuous and interrupted turning process of Ti6Al4V are investigated. Based on the observation of the cutting forces with the different coolant supply strategies, the mean friction coefficient in the sliding region at the tool–chip interface has been obtained and used in a finite element method (FEM) to simulate the deformation process of Ti6Al4V during turning. From the FEM simulation and Oxley's predictive machining theory, cutting forces have been estimated under different coolant supply strategies and verified experimentally.

Keywords Minimum quantity of lubricant · Cutting force model · Finite element method · Flood coolant

Z. G. Wang (✉)
Department of Mechanical and Aeronautical Engineering,
University of California, Davis,
One Shields Avenue,
Davis, CA 95616, USA
e-mail: zgwang@ucdavis.edu

M. Rahman · Y. S. Wong · K. S. Neo · J. Sun · C. H. Tan
Department of Mechanical Engineering,
National University of Singapore,
10 Kent Ridge, Crescent,
Singapore 119260, Singapore

H. Onozuka
Production Engineering Research Laboratory, Hitachi,
Yokohama, Japan

1 Introduction

Interrupted cutting has been used for gear facing, spline shaft turning, etc. Recently, high-speed milling of die and mould steel has been widely used to generate high-quality and intricate sculptured surfaces. Because of the intermittent nature of interrupted cutting, tool wear is usually more severe, and the cutting mechanism is different from continuous cutting. While the application of interrupted cutting has increased, there is relatively little research effort on interrupted cutting of titanium alloy.

Titanium alloys have been widely used in the aerospace, biomedical, automotive, and petroleum industries because of their good strength-to-weight ratio and superior corrosion resistance. However, it is very difficult to machine them due to their poor machinability. Among all titanium alloys, Ti6Al4V is most widely used; therefore, it has been chosen as the workpiece material in this study. When machining Ti6Al4V, conventional tools wear rapidly, because the poor thermal conductivity of Ti6Al4V results in higher temperature closer to the cutting edge during machining, and there exists strong adhesion between the tool and work material [1].

Using a coolant is a reasonable way to improve the machinability of Ti6Al4V. Cutting fluids have often been used to cool and lubricate tool–workpiece and tool–chip interface, and they can also extend the tool life and improve the machined surface quality. However, cutting fluids are difficult and expensive to recycle. In addition, it has a negative impact on the working environment and human health. Therefore, in order to minimize the consequences of cutting fluids, it is important to find a way to accomplish the machining purpose without or with little cutting fluid. To achieve this goal, the alternative strategies are minimal quantities of lubricants (MQL) and dry cutting (DC).

Table 1 Mechanical properties of Ti6Al4V

Tensile strength	Yield strength	Poisson's ratio	Modulus elasticity	Hardness (HRC)
993 MPa	830 MPa	0.342	114 GPa	HRC-36

Weinert et al. [2] discussed the effects of the elimination of or significant reduction in the coolant on all components of a production system. A detailed overview on means to ensure an efficient process and enable dry machining successfully is also given in [2]. MQL means only tiny quantities of a coolant are fed to the cutting process. With the use of very small amount of water and soluble oil, MQL utilizes a compressed air stream to form an oil mist that is directed at the cutting edge. The fine oil mist is able to get close to the tool–chip and tool–workpiece interface, thereby reducing friction and cutting forces generated during machining. Temperature reduction at the cutting zone is achieved by its evaporation and vaporization, which differs from flood coolant (FC) application. Rahman et al. [3, 4] used MQL in end milling of ASSAB 718HH steel and concluded that the MQL technique can be adopted as a replacement of DC, and it may also be an alternative economic approach for FC. Wakabayashi et al. [5] also used the MQL technique in the turning process. They found that MQL provided satisfactory cutting performance compared with the conventional FC. In this paper, the three coolant supply strategies, FC, DC with high-pressure air, and MQL, used in the turning process of Ti6Al4V are investigated.

Numerous cutting force models have been established to predict the machining parameters. Most focused primarily on DC conditions, although coolants are widely used in practical machining, especially for difficult-to-cut materials, such as Ti6Al4V. For finite element method (FEM) simulation of machining, one of the main problems is to determine the boundary conditions at the tool–chip interface. The presence of the coolant makes it extremely difficult to determine the friction coefficient at the tool–chip interface. The main purpose of this paper is to investigate the effects of these coolant supply methods on the cutting forces. Firstly, orthogonal cutting experiments were carried out to determine the friction conditions under the different coolant supply strategies. Then, the friction conditions were incorporated into the FEM simulations to estimate cutting forces.

2 Experimental setup

2.1 Workpiece materials

The work material used in this study is an α–β titanium alloy Ti6Al4V, and its properties are shown in Table 1. A Ti6Al4V pipe with an inner diameter of 43.5 mm and an outer diameter of 49.5 mm was used as the workpiece, as shown in Fig. 1a. In order to obtain interrupted cutting, axial 5-mm-width slots were premachined on its cylindrical surfaces, as shown in Fig. 1b–d. One, two, and four slots were tried. The number of slots together with the spindle rotation speed determined the frequency of interruption.

2.2 Cutting tool materials

Uncoated carbide (WC) inserts were used in this study, whose ISO number is TNGA-160404 [6]. The tool material H1 (Sumitomo's tool material reference number) has fine-carbide grain and maintains high wear resistance. The mechanical properties of H1 are given in Table 2 [6], including the properties of CBN and ceramic materials from [7], cited to highlight the fracture toughness of cemented carbide H1, where H_V: Vickers hardness, k: thermal conductivity, ν: Poisson's ratio, E: Young's modulus, and K_{IC}: fracture toughness. Table 2 shows that cemented carbide H1 has higher transverse rupture strength (TRS) value and fracture toughness, although its hardness value is lower. In addition, cemented carbide tools are much cheaper than CBN and ceramic tools. Therefore, the higher TRS value and greater thermal conductivity of H1 make it more suitable for interrupted cutting.

2.3 Machining tests and cutting conditions

All experiments were carried out on an Okuma CNC lathe machine with 10 kW power and maximum rotation speed of 2,500 rpm. The test conditions for measuring the cutting

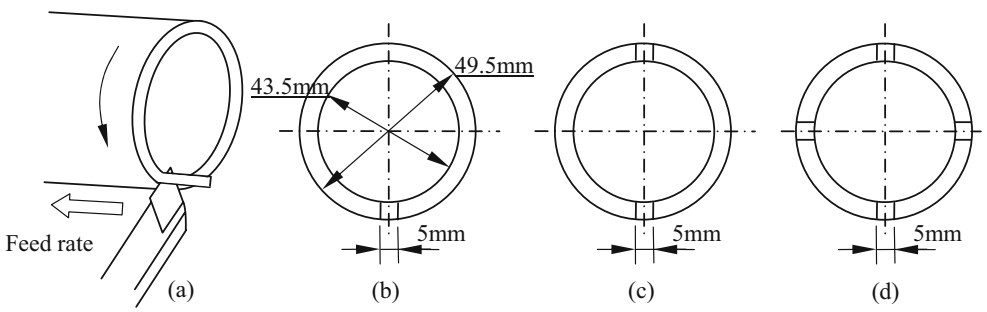

Fig. 1 Orthogonal turning process

Table 2 Properties of CBN, H1, and ceramic tool

Materials	HV (GPa)	TRS (GPa)	k (W/m K)	v	E (GPa)	KIC (MPa/m)
CBN	35–40	1.40	100–130	0.2–0.22	600–800	3.5–6.7
H1 (5% Co)	16.05	*2.06*	109	0.22	646	*10.9*
Ceramic (Si3N4)	21.58	0.793	29	0.26	338	6.2

forces are listed in Table 3. The cutting inserts were mounted on a KISTLER dynamometer 9121 to measure the cutting forces. The force signals were subsequently amplified by a KISTLER charge amplifier and then captured and stored in a computer via an analogue/digital interface. In each experiment, a new cutting edge of the insert was used and the experiments were repeated twice to reduce experimental error at all cutting conditions.

In this study, Ecocool SCO-5, a fully synthetic water-soluble coolant containing glycol as the lubricity agent, was used as the FC in a volumetric concentration of 1:20. In flood cooling, a large amount of the coolant is flushed at the cutting zone at a low pressure so as to remove the generated cutting heat. It is based on the assumption that the greater the amount of lubricant, the better is the cutting process. However, its effectiveness is only limited to lower-speed conditions [8]. Ebara Atomizer was used to generate the ultrafine droplets of oil mist, and vegetable oil was used in the MQL technique.

3 Modeling of orthogonal cutting process

The widely used shear plane model was first proposed by Merchant [9], based on the assumption of continuous chip formation in a narrow zone which is idealized as a plane with uniformly distributed shear stress. Considering the dependence of flow stress of metal on strain, strain rate, and temperature, Oxley [10] developed a more effective model, which considered the variation of flow stress properties in terms of the strain, strain rate, and temperature. This model assumes a thin shear zone, chip equilibrium, and uniform shear stress in the secondary deformation zone at the tool–chip interface. According to Oxley's theory, the forces in chip formation are illustrated in Fig. 2, where t_1 is the undeformed chip thickness, t_2 is the chip thickness, α is the rake angle, ϕ is the shear angle, and β is the friction angle at the tool–chip interface. The area between the boundary CD and EF is the chip formation zone or the shear zone.

Table 3 Summary of cutting conditions

Condition	
Cutting speed (m/min)	60, 75, 90, 105, 120
Feed rate (mm/r)	0.10, 0.15
Clearance angle (degrees)	5
Rake angle(degrees)	−5
Cooling method	Dry, FC, MQL

According to the geometric relations shown in Fig. 2, the following equations can be obtained:

$$\tan\phi = \frac{(t_1/t_2)\cos\alpha}{1-(t_1/t_2)\sin\alpha} \tag{1}$$

$$\beta = \alpha + \arctan(F_t/F_c) \tag{2}$$

$$\begin{aligned}\tau &= F_R\cos(\phi+\beta-\alpha)/A_s \\ &= \sqrt{F_t^2+F_c^2}\cos(\phi+\beta-\alpha)/(bt_1/\sin\phi)\end{aligned} \tag{3}$$

where b is the width of cut and A_s is the area of the shear plane.

When the chip thickness ratio is known, the shear angle ϕ can be estimated from Eq. 1. However, it is very difficult to estimate the friction accurately, especially when different coolant supply methods are used. After the shear angle and friction angle are obtained, the shear stress along the shear plane AB can be estimated with Eq. 3 based on experimentally obtained cutting and thrust forces.

3.1 Determination of friction forces at tool–chip interface

At the tool–chip interface, Zorev [11] assumed that two regions exist: sticking region and sliding region, as shown in Fig. 3. In the sticking region, the uniformly distributed shear frictional stress is equal to the local shear flow stress. In the sliding region, Coulomb's friction law can be applied. An appropriate estimate for the friction coefficient was experimentally determined according to the friction angle.

3.2 Modeling of flow stress properties of Ti6Al4V

The yield stress of a metal under uniaxial conditions is defined as the flow stress or effective stress. The metal starts deforming plastically when the applied stress reaches the value of the flow stress [12]. The flow stress is mostly influenced by temperature, strain, strain rate, and material properties. Accurate and reliable flow stress models are very important for describing the deformation behavior of the work material during practical machining processes.

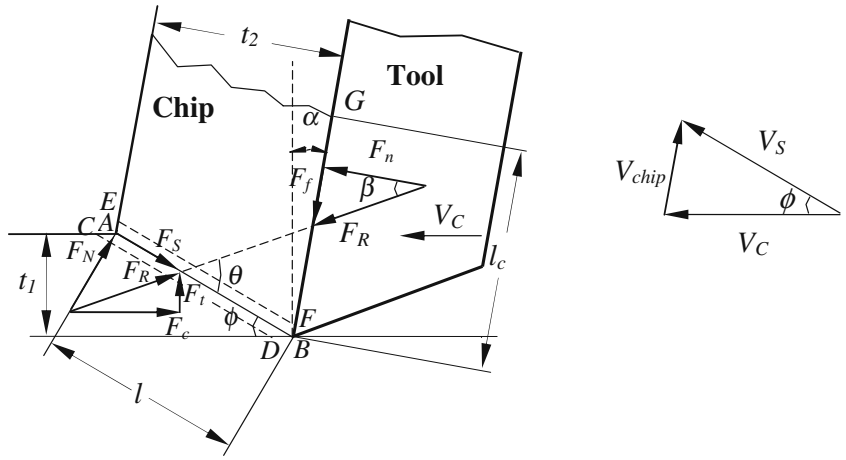

Fig. 2 Cutting forces diagram based on the shear plane model

The widely used constitutive model of flow stress is the JC strength model proposed by Johnson and Cook [13]. The JC model represents the flow stress $\overline{\sigma}$ of a material as the product of strain, strain rate, and temperature, as shown in Eq. 4.

$$\overline{\sigma} = [A + B(\overline{\varepsilon})^n]\left[1 + C\ln\left(\frac{\dot{\overline{\varepsilon}}}{\dot{\overline{\varepsilon}}_0}\right)\right]\left[1 - \left(\frac{T - T_r}{T_m - T_r}\right)^m\right] \quad (4)$$

The parameter A is the initial yield strength of the material at room temperature and at a strain rate of 1 s^{-1}; $\overline{\varepsilon}$ is the equivalent plastic strain; $\dot{\overline{\varepsilon}}$ is the strain rate normalized by a reference strain rate $\dot{\overline{\varepsilon}}_0$. The temperature term is valid within the range from room temperature (T_r) to melting temperature of the work material (T_m). The parameters B, C, m, and n are fitted to the experimental results obtained from corresponding compression and tension tests. This model can be calibrated more easily. Therefore, some researchers chose the JC model as constitutive equation for deformation behavior of metals at higher strain rate and high temperature. Based on the published flow stress data of Ti6Al4V, Wang et al. [14] estimated the parameters for the JC model with the Gauss–Newton algorithm, and the estimated values for these parameters have also been used in this study for FEM simulation.

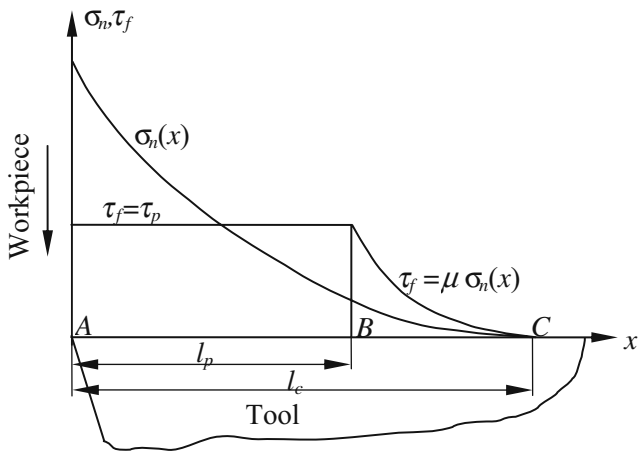

Fig. 3 Curves representing normal stress (σ_n) and frictional stress (τ_f) distributions on the tool rake face proposed by Zorev [11]

3.3 FEM simulation of orthogonal turning

Ozel and Altan [12, 15] have done much definitive works in the use of FEM to simulate the cutting process. They developed a predictive model for high-speed milling based on FEM simulations. They used the model to predict the resultant cutting forces, flow stresses and temperatures primarily in turning and flat end milling. They indicated that there are two major unknown parameters: shear flow stress of the chip k_{chip} and the constant friction coefficient μ_p. From the JC model of Ti6Al4V, the shear flow stress of the chip can be estimated. In practical simulation, an initial value of μ_p is assumed at the start of the simulation. In this study, the initial value of μ_p was calculated with Eq. 2 using the measured cutting forces.

The coolant supply strategy will not only affect the friction coefficient but also the convective heat transfer coefficient between the tool and workpiece combination. Based on the published data given in [16], the heat transfer coefficient value of 22.6 W/m^2 °C was set as the initial value at the start of the simulation under MQL condition.

4 Results and discussion for continuous cutting

4.1 Results and discussion about friction angles

The cutting forces (F_c) in the cutting direction and thrust force (F_t) in the feed direction as shown in Fig. 2 were measured during orthogonal turning of Ti6Al4V. After getting the values of F_c and F_t, the mean values of the

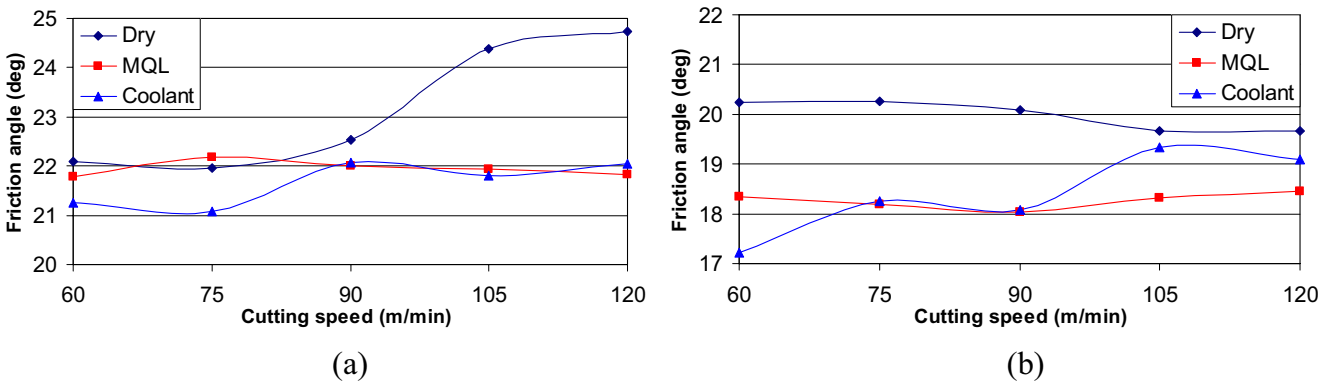

Fig. 4 Friction angles in continuous cutting. **a** Friction angle at the feed rate of 0.10 mm/r. **b** Friction angle at the feed rate of 0.15 mm/r

friction angles at the feed rate of 0.10 and 0.15 mm/r can be calculated from Eq. 2 as shown in Fig. 4. In [17], it was found that thrust forces under DC are much higher than those under MQL and FC at higher cutting speed. These higher thrust forces at higher cutting speed cause the increase in the friction angle under DC conditions. For all the cutting conditions, friction angles under MQL are only slightly different from those under FC. This demonstrates that MQL and FC may have similar effective lubrication and cooling ability at the low feed rate. Since at a low feed rate, less cutting heat is generated, MQL and FC are effective enough to cool the tool and lubricate the tool/chip interface.

When the feed rate is increased to 0.15 mm/r, more workpiece materials are removed than those at lower feed rate within the same machining time; therefore, the tool undergoes a larger cutting load. Under this condition, the ineffective cooling and lubrication capacity provided by DC is much more obvious. For all of the same cutting conditions, the friction angles under MQL and FC are much smaller than those under DC. The reason for this may be that inadequate lubrication and cooling ability for DC results in higher temperature at the cutting region. Finally, the higher temperature affects the physical properties of the cutting tool and results in an increase in the thrust force in comparison to the other two coolant supply strategies. In addition, at the cutting speed greater than 90 m/min, the friction angle under MQL is smaller than that under FC, so MQL seems to be more effective than FC. At a higher cutting speed, except for cooling ability, MQL has better lubrication ability than FC, as shown in Fig. 4b. This lower friction coefficient enables the chips to flow much easier away from the rake face.

4.2 Chip morphology

According to the popular chip form classification developed by ISO [18], chip types usually have the following forms: straight ribbon, tubular, corkscrew (washer), and conical helical. Based on this definition, chips obtained in this study are tubular. Among the chip morphologies listed in Figs. 5, 6, and 7, some chips obtained under MQL are long, as shown in Fig. 6, and others from DC and FC become snarled, as shown in Figs. 5 and 7b–d. This may come from the different normal forces acting on the tool–chip interface.

Figure 8 shows that at low cutting speed, normal forces under MQL are larger than those under DC and FC. These slightly larger normal forces may modify the deformation pattern within the chip formation zone and consequently the chip form as the chip leaves the cutting zone. This is the reason why the chip forms under MQL at low cutting speed are different from those under DC and FC at the same cutting speed. At low cutting speed under MQL, chips are long, but for DC and FC, chips become snarled, as shown in Figs. 5, 6, and 7.

In this study, the chip thickness has also been measured with the micrometer, as shown in Fig. 9. At the feed rate of 0.10 mm/r, the chip thickness increases with the cutting

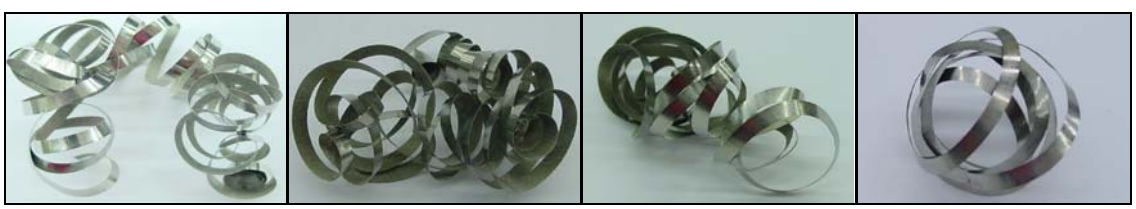

Fig. 5 Chip morphologies under DC (feed rate=0.10 mm/r). **a** v=75 m/min, **b** v=90 m/min, **c** v=105 m/min, **d** v=120 m/min

Fig. 6 Chip morphologies under MQL (feed rate=0.10 mm/r). **a** v=60 m/min, **b** v=75 m/min, **c** v=90 m/min, **d** v=105 m/min

speed, as shown in Fig. 9a. Under a specific tool/workpiece combination and a certain undeformed chip thickness, the chip thickness depends on the cutting speed and cutting temperature. At a low feed rate, the chip thickness is thinner. In addition to cooling and lubrication abilities, another main function of cutting coolants is to carry the chips away from the cutting zone. Under the effect of high-pressure air coolants and FCs, it may remove chips within a shorter time, and it causes a larger amount of heat to be taken away by chips. Thus, chips do not have enough time to deform plastically. Finally, the chips under higher cutting speed become more difficult to deform and then result in the increase in chip thickness. Under MQL and DC, the chip thickness gradually decreases with the increase in the cutting speed at the feed rate of 0.15 mm/r. Because at higher feed rate, more cutting heat is generated during machining with the increase in cutting speed within the same machining time, this higher cutting heat may make chips deform easier. Finally, it results in the decrease in chip thickness with the increase in cutting speed. However, there is no obvious trend to describe the effect of FC on the chip thickness. This may be due to unstable cooling capability of FC during continuous cutting, especially at high cutting speed.

4.3 Results and discussion about shear angle and shear stress

After getting the chip thickness, the shear angle can be estimated with Eq. 1; then, shear stress can be predicted further with Eq. 3. Figure 10 presents the estimated shear angles and shear stresses when the feed rate is equal to 0.10 and 0.15 mm/r, respectively. At the feed rate of 0.10 mm/r, shear angles decrease with the increase in the cutting speed as shown in Fig. 10a. The reason for this is that chip thickness increases with the cutting speed, as shown in Fig. 9a. And, according to Eq. 1, the shear angle decreases with the increase in the chip thickness. However, when feed rate= 0.15 mm/r, under MQL and DC, the shear angle increases with the cutting speed. The reason for this is that the chip thickness decreases with the cutting speed under MQL and DC. But, under FC, the shear angle first increases with the cutting speed and then decreases with the further increase in the cutting speed. This may be due to the instable cooling ability of FC. Under DC, the values of the shear stress are less than those under MQL and FC. This is because high cutting temperature under DC makes it much easier to remove the work material.

5 Results and discussion for interrupted cutting

5.1 Results and discussion about friction angles

Figure 11 presents friction angles for interrupted cutting. In interrupted cutting, there are cutting and noncutting durations. Under drying cutting, the friction angle in one-slot interrupted cutting is smaller than that in continuous cutting at the same cutting parameters. During the non-cutting period, higher cutting temperature at the insert could be cooled down. Thus, it is possible that the cutting tool may not have reached saturated temperature. Therefore, it may help the insert to restore hardness and other properties. The higher thermal conductivity of H1 may also contribute to better endurance to interrupted cutting as the tool may gain more temperature drop during the noncutting period

Fig. 7 Chip morphologies under FC (feed rate=0.10 mm/r). **a** v=60 m/min, **b** v=75 m/min, **c** v=105 m/min, **d** v=120 m/min

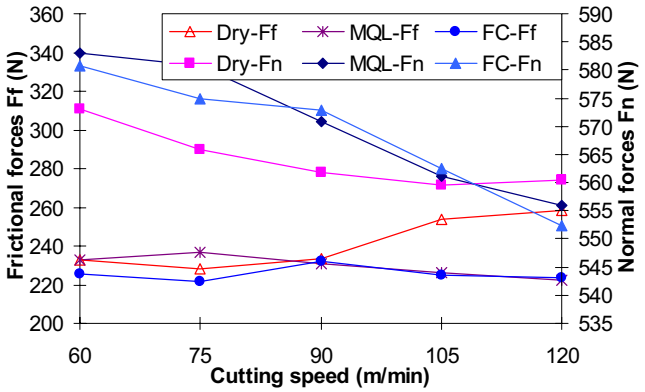

Fig. 8 Frictional and normal forces in continuous cutting (feed rate= 0.10 mm/r)

and restore hardness. In interrupted cutting, with the feed rate of 0.10 mm/r, FC does not show any obvious improvement in comparison to MQL and DC. Therefore, FC is not as effective in one-slot interrupted cutting as that in continuous cutting.

In one-slot interrupted cutting, at a higher feed rate of 0.15 mm/r, the friction angle in DC at the cutting speed greater than 90 m/min is higher than that under MQL and FC. This may be attributed to the reducing cooling ability of high-pressure air at higher cutting speed. Because at higher feed rate and higher cutting speed, a larger amount of heat is generated due to larger volume removal rate, high-pressure air is inadequate to lubricate and cool down the tool–chip interface. At a higher feed rate of 0.15 mm/r and higher cutting speed, MQL and FC have similar effects on the friction angle. This reiterates that MQL is an effective alternative approach for FC.

When the number of slots is increased to two at the feed rate of 0.15 mm/r, the experimental value of the friction angle at higher cutting speed under FC is larger than that under DC and MQL. During noncutting duration, the strong cooling ability of FC is more likely to result in larger amplitude of temperature change. The alternating temperature change cycle results in higher temporal temperature gradient on the cutting edge. Normally, the cyclic temperature gradient causes thermal stress called "thermal shock," which is the main mechanism of thermal cracking. From SEM figures listed in Fig. 12, there are some chippings at the cutting edge under FC, as shown in Fig. 12e,f. This indicates that FC is not an effective alternative approach for interrupted cutting. Similar phenomena have also been observed by Chou and Evans [19]. Under DC and MQL, no crack was observed on the rake faces, as shown in Fig. 12a–d. Compared to DC, MQL is more efficient since a smaller friction angle under MQL is obtained than that under DC.

In interrupted cutting, the workpiece with four slots, as shown in Fig. 1d, was also tried. However, the inserts wore out quickly, and this resulted in much increase in the cutting forces. In interrupted cutting, both mechanical and thermal loads affect tool wear. In four-slot interrupted cutting, the frequency of interruption is higher, and the mechanical impact and thermal shock with higher frequency are detrimental to tool life. The high frequency thermal load may cause thermal cracking, and the mechanical impact can result in microfracture at the cutting edge. Figure 13 suggests that there exist cracks and chippings at the cutting edge for the four-slot interrupted cutting. Thus, H1 inserts are not suitable for interrupted cutting with higher interruption frequency.

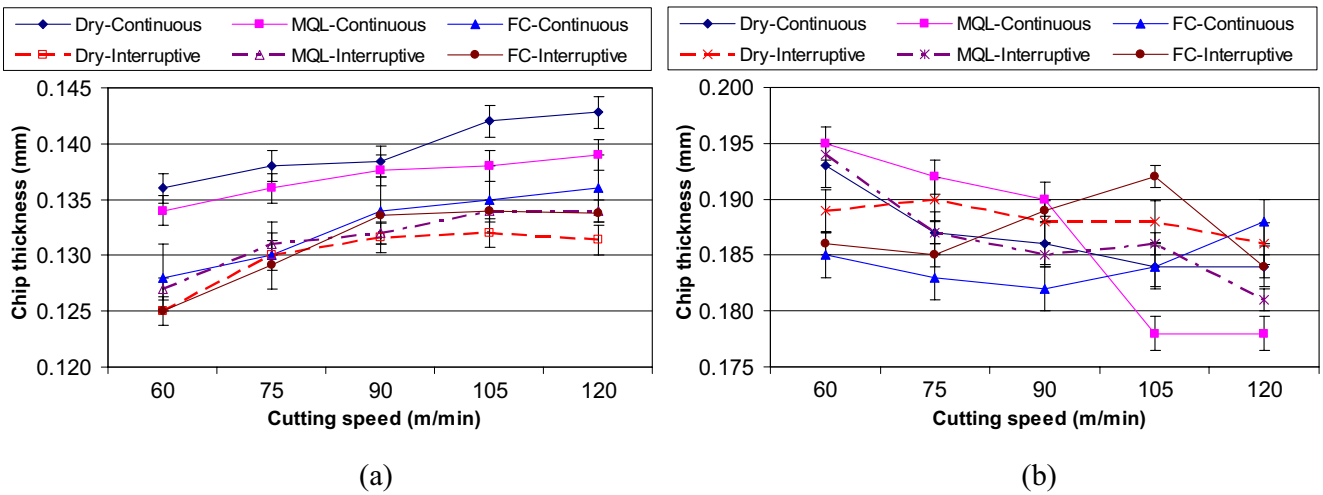

Fig. 9 Chip thickness at different cutting conditions. **a** Chip thickness at the feed rate 0.10 mm/r, **b** chip thickness at the feed rate 0.15 mm/r

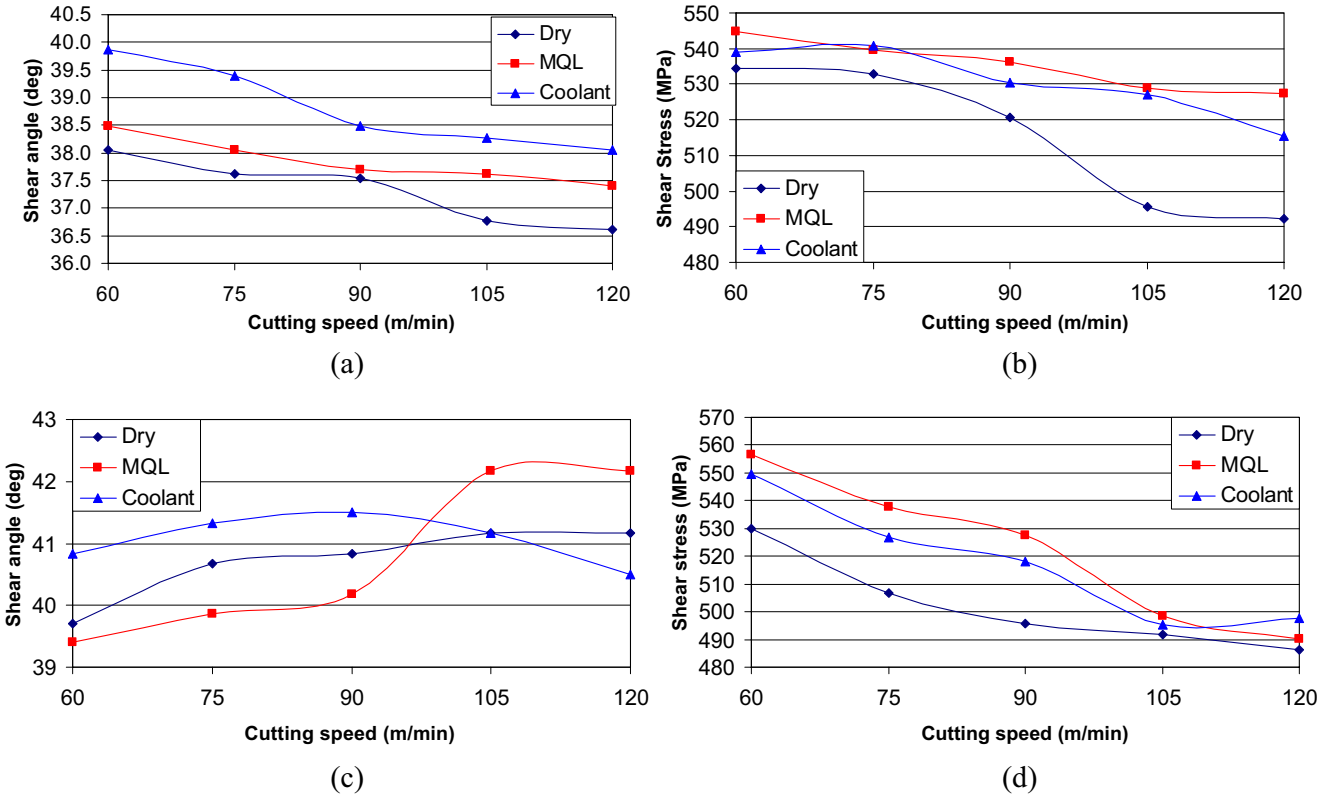

Fig. 10 Shear angle and shear stress in continuous cutting. **a** Shear angle at the feed rate of 0.10 mm/r. **b** Shear stress at the feed rate of 0.10 mm/r. **c** Shear angle at the feed rate of 0.15 mm/r. **d** Shear stress at the feed rate of 0.15 mm/r

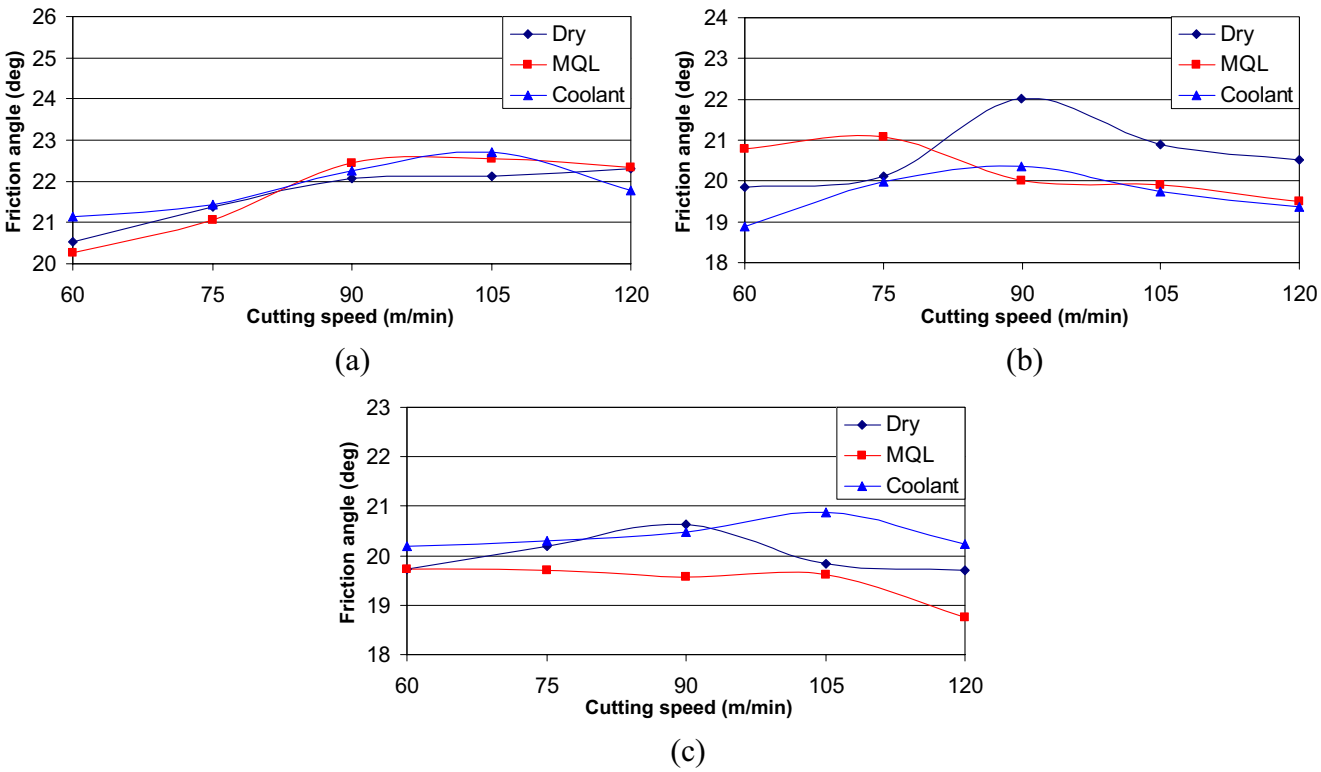

Fig. 11 Friction angles in interrupted cutting. **a** Feed rate=0.10 mm/r, one-slot, **b** feed rate=0.15 mm/r, one-slot, **c** feed rate=0.15 mm/r, two-slot

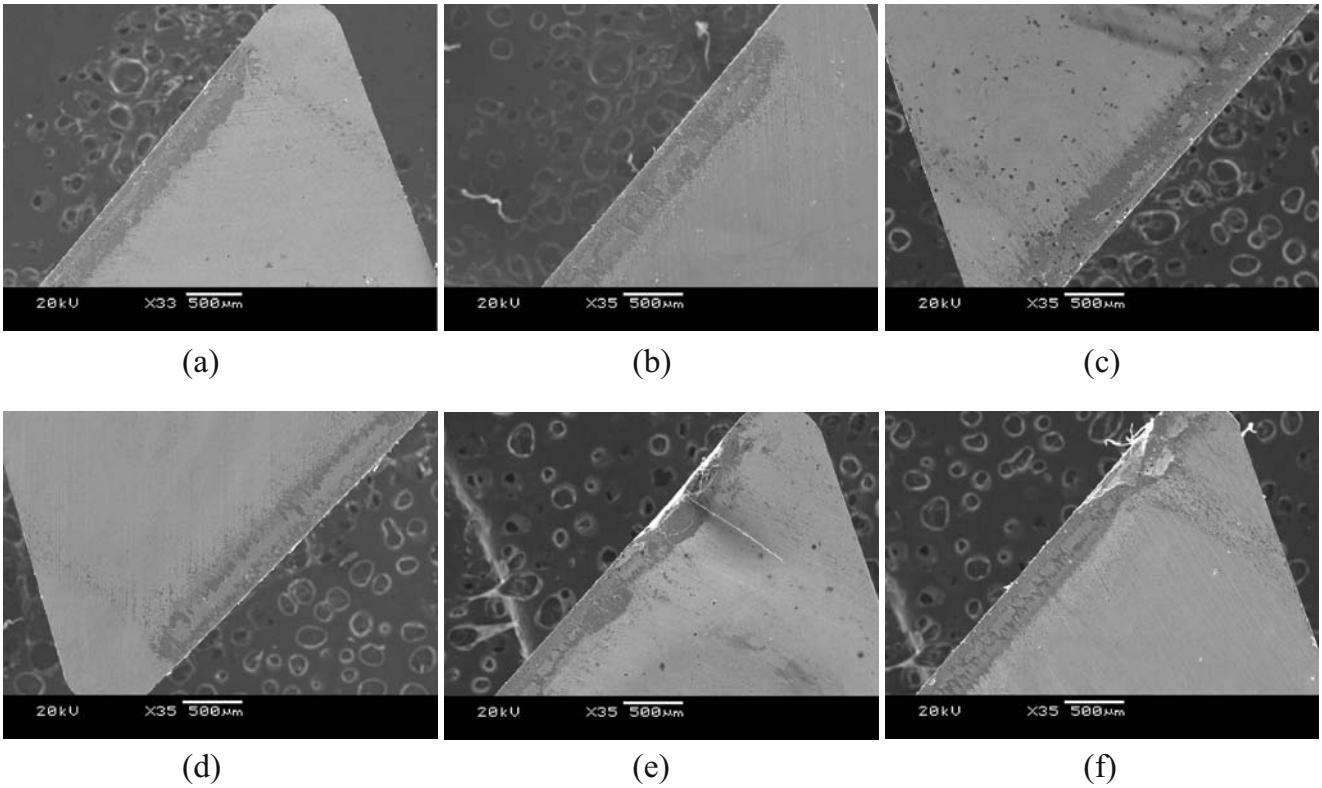

Fig. 12 SEM of the rake faces in two-slot interrupted cutting (feed rate=0.15 mm/r). **a** v=60 m/min under DC; **b** v=90 m/min under DC; **c** v=75 m/min under MQL; **d** v=105 m/min under MQL; **e** v=75 m/min under FC; **f** v=90 m/min under FC

5.2 Results and discussion about shear angle and shear stress

As described in Section 4.3, the shear angle and shear stress in interrupted cutting can also be predicted with Eqs. 1 and 3, as shown in Figs. 14, 15, and 16.

At the feed rate of 0.10 mm/r, the shear angle and shear stress decrease with the increase in the cutting speed at the cutting speed of less than 120 m/min. However, when the feed rate=0.15 mm/r, for one-slot interrupted cutting under MQL and DC, the shear angle tends to increase with the cutting speed, but it does not show any obvious trend with the increase in cutting speed under FC because of its unstable cooling ability.

For two-slot interrupted cutting when cutting speed is greater than 60 m/min, the shear angle increases with the cutting speed. Under MQL and DC, the shear angle in two-slot interrupted cutting shows a similar trend as that in one-slot interrupted cutting.

During all interrupted cutting, the shear stress has a similar trend to decrease with the increase in cutting speed.

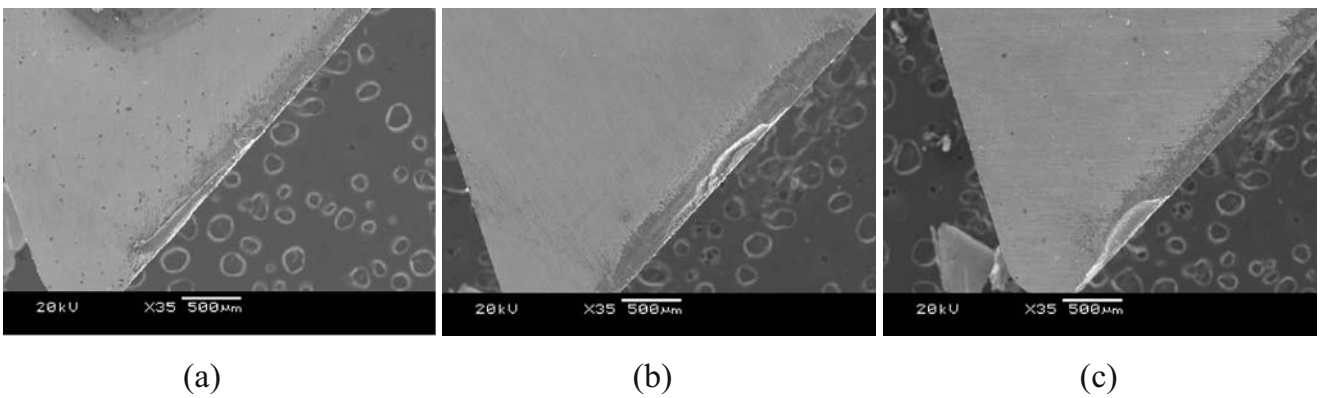

Fig. 13 SEM of the rake faces in four-slot interrupted cutting (feed rate=0.15 mm/r). **a** v=75 m/min under MQL, **b** v=90 m/min under MQL, **c** v=120 m/min under MQL

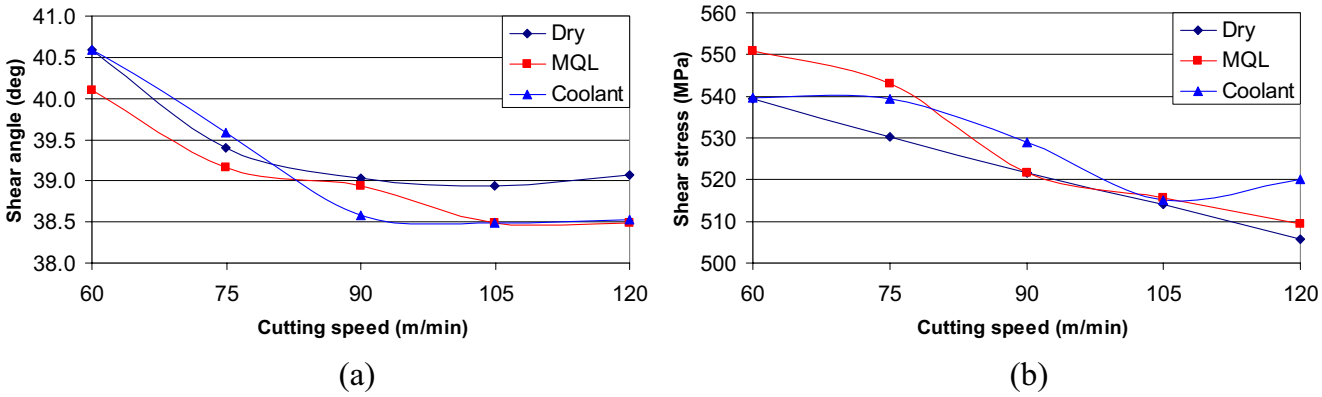

Fig. 14 Shear angle and shear stress in one-slot interrupted cutting (feed rate=0.10 mm/r). **a** Shear angle, **b** shear stress

5.3 Estimation of cutting forces

Using the determined friction data, the value of heat-transfer coefficient, and JC model of Ti6Al4V, process simulations have been conducted. The simulation of plastic deformation of chip formation when machining Ti6Al4V is shown in Fig. 17. There exists an obvious deformation zone as indicated in Fig. 17, which is also called the chip formation zone.

Using the determined friction data and JC model of Ti6Al4V, FEM simulations can be carried out repeatedly. In FEM simulation under different conditions, the values of the shear angle ϕ are found by fitting the maximum strain rate along the thin shear zone, and simultaneously, the position of shear plane AB can be determined. Then, the shear stress k_{AB} can be estimated based on the position of shear plane AB. In addition, the value of friction angle β can also be obtained from the simulation results. Finally, the cutting forces are found from the geometrical relationships given in Fig. 2a. With this procedure, the cutting forces can be calculated accurately and realistically.

The predicted and experimental cutting forces are presented in Fig. 18. Under DC conditions, at the cutting speed of 120 m/min, the estimated cutting force has a larger difference from the experimental one, but the prediction error is still within 10%. More importantly, for other cases, the estimated values of cutting forces and thrust forces are only slightly different from the experimental ones. Therefore, after incorporating the sophisticated friction conditions at the tool–chip interface, FEM simulation can predict the cutting and thrust forces with good accuracy. With the same procedure, cutting forces and thrust forces can also be predicted for other cutting conditions.

6 Conclusions

In this paper, cutting performances in continuous and interrupted cutting have been investigated under DC, MQL, and FC. FEM is also used to simulate the orthogonal turning process. The following conclusions have been drawn:

1. In continuous cutting, DC has been found to be only effective at lower cutting speed and feed rate. MQL and FC have similar cooling and lubrication ability. At higher cutting speed and high feed rate, MQL seems to be more effective than FC, because of its better lubrication ability.

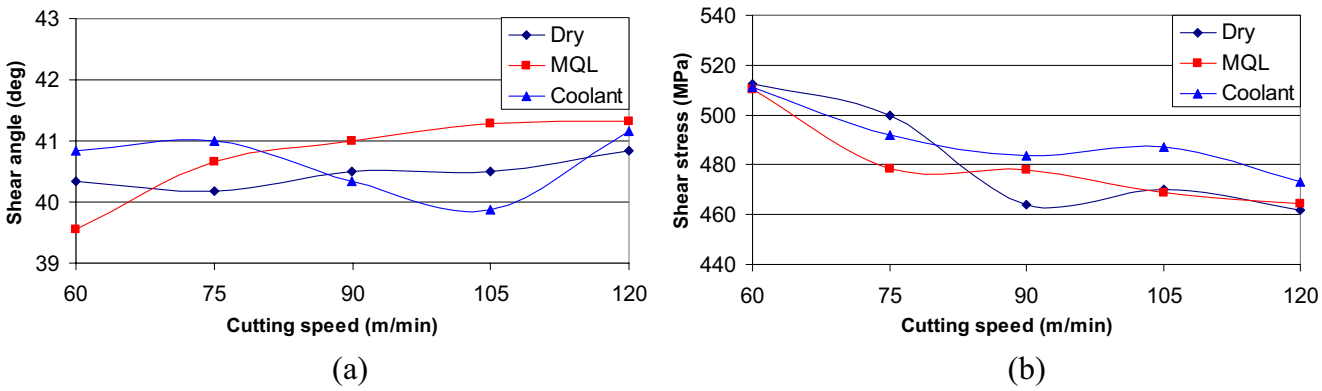

Fig. 15 Shear angle and shear stress in one-slot interrupted cutting (feed rate=0.15 mm/r). **a** Shear angle, **b** Shear stress

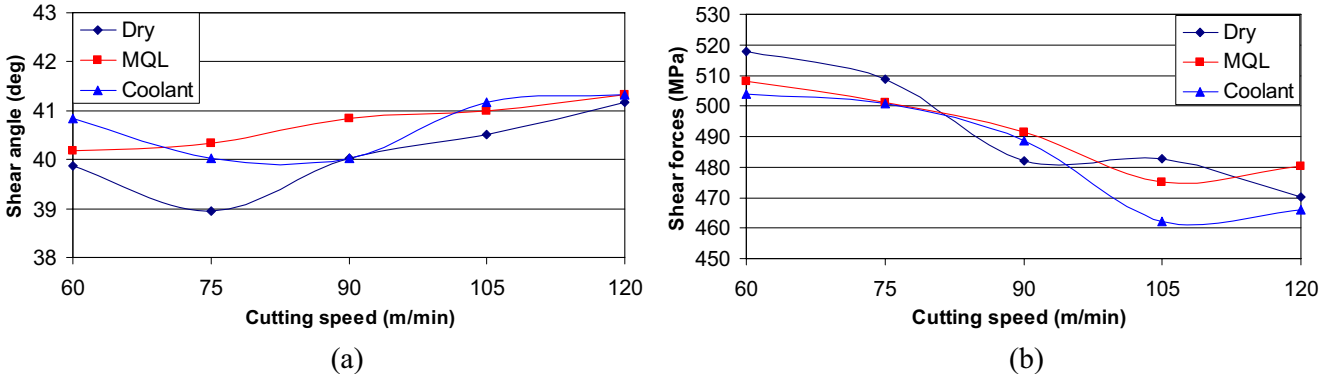

Fig. 16 Shear angle and shear stress in two-slot interrupted cutting. **a** Shear angle at the feed rate of 0.15 mm/r, **b** Shear stress at the feed rate of 0.15 mm/r

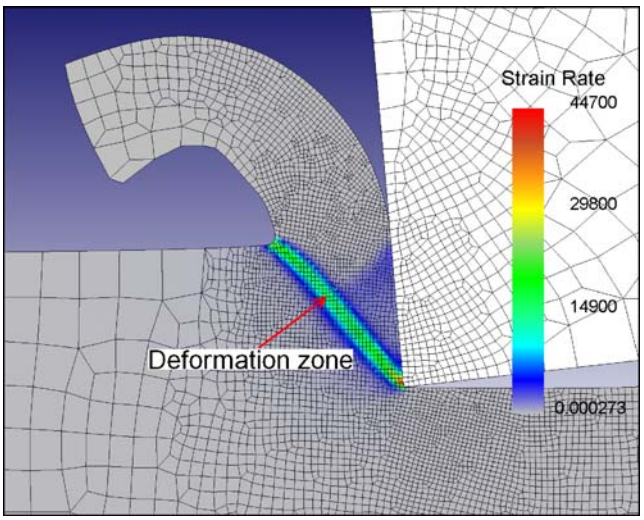

Fig. 17 Deformation zone of FEM simulation in machining of Ti6Al4V

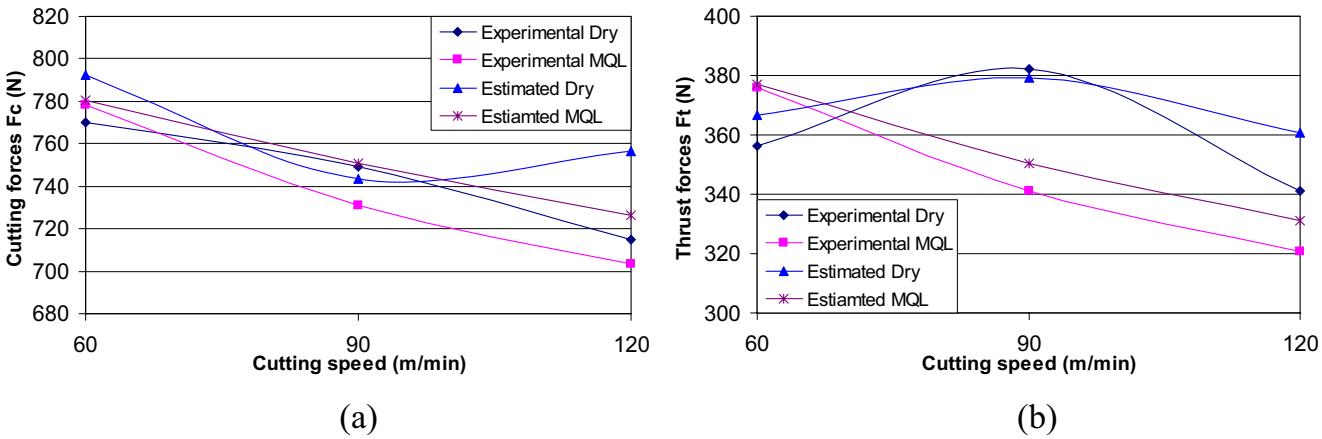

Fig. 18 Estimated and experimental forces in one-slot interrupted cutting. **a** Cutting forces at the feed rate of 0.10 mm/r, **b** thrust forces at the feed rate of 0.10 mm/r

2. In interrupted cutting, MQL is more effective than DC and FC, especially in two-slot interrupted cutting. Thus, MQL is a more economical alternative cooling lubricant than FC.
3. H1 carbide tools are suitable for one-slot and two-slot interrupted cutting. For the four-slot interrupted cutting, H1 inserts wear out quickly under higher frequency of mechanical and thermal loading.
4. Based on the experimental results, the mean friction angles at the tool–chip interface have been determined. The JC model is used to describe the deformation behavior of Ti6Al4V during orthogonal cutting. In the proposed model, a more sophisticated friction model at the tool–chip interface is incorporated. Then, orthogonal turning of Ti6Al4V is simulated with FEM based on the constitutive model for Ti6Al4V. From the FEM simulation results, cutting and thrust forces in orthogonal cutting have been estimated. Comparison between the experimental and estimated forces shows that cutting and thrust forces have been predicted with good accuracy.

References

1. Zoya ZA, Krishnamurthy R (2000) The performance of CBN tools in the machining of titanium alloys. J Mater Process Technol 100:80–86 doi:10.1016/S0924-0136(99)00464-1
2. Weinert K, Inasaki I, Sutherland JW, Wakabayashi T (2004) Dry machining and minimum quantity lubrication. CIRP Ann 53 (2):511–537
3. Rahman M, Kumar AS, Salam MU (2001) Evaluation of minimal quantities of lubricant in end milling. Int J Adv Manuf Technol 18 (4):235–241 doi:10.1007/s001700170063
4. Rahman M, Kumar AS, Salam MU (2002) Experimental evaluation on the effect of minimal quantities of lubricant in milling. Int J Mach Tools Manuf 42(5):539–547 doi:10.1016/S0890-6955(01)00160-2
5. Wakabayashi T, Inasaki I, Suda S, Yokota H (2003) Tribological characteristics and cutting performance of lubricant esters for semi-dry machining. CIRP Ann 52(1):61–64
6. Sumitomo Electric Industries (2000) Performance cutting tools. Sumitomo Electric Industries, Japan
7. Sandvik Hard Materials (2001) Cemented carbide rod blanks for metal cutting. Sandvikens Tryckeri, Sweden
8. Paul S, Chattopadhyay AB (1995) Effects of cryogenic cooling by liquid nitrogen jet on forces, temperature and surface residual stresses in grinding steels. Cryogenics 35(8):515–523 doi:10.1016/0011-2275(95)98219-Q
9. Merchant ME (1944) Basic mechanics of the cutting process. ASME J Appl Mech 67:168–175
10. Oxley PLB (1989) The mechanics of machining: an analytical approach to assessing machinability. E. Horwood, Chichester, UK
11. Zorev NN (1963) Interrelationship between shear processes occurring along tool face and on shear plane in metal cutting. In: Proceedings of the Conference on International Research in Production Engineering, ASME, New York, pp 42–49
12. Ozel T (1998) Investigation of high speed flat end milling process: prediction of chip formation, cutting forces, tool stresses and temperatures. Ph.D. thesis, The Ohio State University, Columbus, OH
13. Johnson GR, Cook WH (1983) A constitutive model and data for metals subjected to large strains, high strain rates and high temperatures. In: Proceedings of the 7th International Symposium on Ballistics, The Netherlands, pp 541–547
14. Wang ZG, Rahman M, Wong YS, Li XP (2005) A hybrid cutting force model for high-speed milling of titanium alloys. CIRP Ann 54(1):71–74
15. Ozel T, Altan T (2000) Process simulation using finite element methodx—prediction of cutting forces, tool stresses and temperatures in high-speed flat end milling. Int J Mach Tools Manuf 40 (5):713–738 doi:10.1016/S0890-6955(99)00080-2
16. Kops L, Arenson M (1999) Convective heat transfer coefficients in turning. In: Proceedings of the 15th Brazilian Congress of Mechanical Engineering, Sao Paulo, Brazil, CD-ROM
17. Wang ZG, Rahman M, Wong YS et al (2005) Modeling of cutting forces during machining of titanium alloys with different coolant strategies. In: Proceedings of the 8th CIRP International Workshop on Modeling in Machining Operations, Chemnitz, Germany, pp 275–282
18. ISO (1977) Tool-life testing with single-point turning tools, ISO 3685:1977, Annex G, 41
19. Chou YK, Evans CJ (1999) Cubic boron nitride tool wear in interrupted hard cutting. Wear 225–229:234–245 doi:10.1016/S0043-1648(99)00012-5